Available online at www.sciencedirect.com

ScienceDirect

MATTER AND RADIATION AT EXTREMES

Matter and Radiation at Extremes 3 (2018) 28–39

www.journals.elsevier.com/matter-and-radiation-at-extremes

Review Article

Optimization of hole-boring radiation pressure acceleration of ion beams for fusion ignition

S.M. Weng [a,b,*], Z.M. Sheng [a,b,c,**], M. Murakami [d], M. Chen [a,b], M. Liu [a,b], H.C. Wang [a,b], T. Yuan [a,b], J. Zhang [a,b]

[a] *Key Laboratory for Laser Plasmas (MoE), School of Physics and Astronomy, Shanghai Jiao Tong University, Shanghai 200240, China*
[b] *Collaborative Innovation Center of IFSA, Shanghai Jiao Tong University, Shanghai 200240, China*
[c] *SUPA, Department of Physics, University of Strathclyde, Glasgow G4 0NG, UK*
[d] *Institute of Laser Engineering, Osaka University, Osaka 565-0871, Japan*

Received 30 April 2017; revised 8 September 2017; accepted 11 September 2017
Available online 13 November 2017

Abstract

In contrast to ion beams produced by conventional accelerators, ion beams accelerated by ultrashort intense laser pulses have advantages of ultrashort bunch duration and ultrahigh density, which are achieved in compact size. However, it is still challenging to simultaneously enhance their quality and yield for practical applications such as fast ion ignition of inertial confinement fusion. Compared with other mechanisms of laser-driven ion acceleration, the hole-boring radiation pressure acceleration has a special advantage in generating high-fluence ion beams suitable for the creation of high energy density state of matters. In this paper, we present a review on some theoretical and numerical studies of the hole-boring radiation pressure acceleration. First we discuss the typical field structure associated with this mechanism, its intrinsic feature of oscillations, and the underling physics. Then we will review some recently proposed schemes to enhance the beam quality and the efficiency in the hole-boring radiation pressure acceleration, such as matching laser intensity profile with target density profile, and using two-ion-species targets. Based on this, we propose an integrated scheme for efficient high-quality hole-boring radiation pressure acceleration, in which the longitudinal density profile of a composite target as well as the laser transverse intensity profile are tailored according to the matching condition.

PACS codes: 52.38.Kd; 52.57.-z; 41.75.Jv; 52.65.Rr; 52.72.+v

Keywords: Laser-driven ion acceleration; Radiation pressure acceleration; Fast ignition; Inertial confinement fusion; High energy density; Hole boring

1. Introduction

Efficient ion beam generation in the interactions of intense laser pulses with matters has attracted increasing attention during the last few decades due to their broad applications in fundamental science, medicine, and industry [1,2]. In contrast to conventional accelerators driven by radio frequency fields, laser-driven ion acceleration can afford an accelerating gradient as high as a few hundreds of GV/m. Profiting from this, future laser-driven ion accelerators shall have the advantages of more compact size, shorter bunch duration, higher particle density of the produced beams over the conventional

* Corresponding author. Key Laboratory for Laser Plasmas (MoE), School of Physics and Astronomy, Shanghai Jiao Tong University, Shanghai 200240, China.
** Corresponding author. Key Laboratory for Laser Plasmas (MoE), School of Physics and Astronomy, Shanghai Jiao Tong University, Shanghai 200240, China.
E-mail addresses: wengsuming@gmail.com (S.M. Weng), z.sheng@strath.ac.uk (Z.M. Sheng).
Peer review under responsibility of Science and Technology Information Center, China Academy of Engineering Physics.

https://doi.org/10.1016/j.mre.2017.09.002

accelerators [3,4]. These advantages are of particular importance to many applications, such as radiography and radiotherapy [5–7], high energy density physics [8,9], fast ion ignition [10] of inertial confinement fusion (ICF) and so on.

In particular, fast ion ignition [10] is an attractive variant of fast ignition of ICF [11] which may greatly save the driver energy and simplify the target fabrication for a future high gain fusion reactor [12]. However, a high-quality high-fluence ion beam is critically required for the fast heating of a precompressed high-density fuel target to a sufficiently high temperature [13]. First, the ion beam should have an energy fluence as high as 1.5 GJ cm^{-2} when arrives at the hotspot [14]. Secondly, the ion beam should have a narrow energy spread (usually $\Delta E/E \leq 20\%$) in the stopping power range (usually a few tens of MeV/u) of the precompressed fuel target in order to suppress the time-of-flight spread and deposit the majority of ion energy into the hotspot [15]. Thirdly, a high laser-to-ion energy conversion efficiency ($\geq$10%) is critically required for economic reasons [10]. Therefore, to date the efficient generation of such a high-quality high-fluence ion beam remains a key challenge.

Stimulated by these prospective applications, a variety of novel schemes have been proposed and refined for laser-driven ion acceleration over the past decades. Most of these schemes can be classified into the following main mechanisms: target normal sheath acceleration (TNSA) [16,17], acceleration at relativistic-induced transparency [18] or break-out-afterburner (BOA) ion acceleration [19], collisionless electrostatic shock acceleration [20–22], Coulomb explosion [23,24], radiation pressure acceleration (RPA) [25–35]. Among these schemes, the TNSA is the most studied mechanism in the experiments, and the proton cut-off energy of 85 MeV with high particle numbers has been recorded in a recent experiment [36]. However, the energy spectra of the accelerated ions in the TNSA usually have quasi-exponential profiles. To get quasi-monoenergetic ion beams, the RPA has been proposed [25–35]. In the RPA, the electrons of a solid target can be coherently pushed forward by the ponderomotive force of an intense circularly polarized (CP) laser pulse, which results in a strong charge-separation field for ion acceleration. According to the thickness of irradiated solid targets, the RPA appears in two distinct modes. If the target is an ultrathin foil, then the ions of this foil can be accelerated continuously as a sail since they move together with the charge-separation field. Theoretically, the ions can be accelerated up to GeV by this light-sail mode of the RPA [25–30]. If the target is a thick enough solid target, then the hole-boring mode of the RPA develops [31–35]. At first, the hole-boring process was extensively investigated as an approach to fast ignition since it allowed the laser pulse penetrating deeper into a precompressed fuel target in the ICF [11,37]. Later, a lot of numerical simulations demonstrated that fast ions can be efficiently produced in the hole-boring process of a CP laser pulse penetration into a thick dense target [31–35].

Compared with other laser-driven ion acceleration schemes, the hole-boring RPA has great potential to generate high-fluence ion beams for fast ion ignition of ICF and even for heavy-ion fusion [10,38–42]. The laser-driven ion acceleration is usually realized via a charge-separation field. In general, the fast electrons generated in laser-plasma interactions will create a double layer [43,44], in which a strong electric field is induced due to the charge separation. If the pulse duration is long enough, the double layer can act as a piston and accelerate the whole micro-foil to a high velocity [45]. The accelerated micro-foil, as a plasma block, is particularly interesting for innovative ignition schemes for ICF, such as block ignition and impact fast ignition [44,46]. With an ultrashort laser pulse and a relatively thick dense target, however, the ion acceleration mainly happens in an extremely narrow charge-separation layer with a thickness of a few microns. Consequently, only the ions at a specific layer can be accelerated. For instance, the ions can be accelerated at the rear surface of a solid target in the TNSA [16,17]. In the hole-boring RPA, however, the ions of a thick solid target can be accelerated layer by layer, and finally a kind of volume acceleration is achieved [47]. Theoretically, such a layer-by-layer acceleration can continuously go on, thus there is no limitation upon the accelerated ion number if the laser pulse and the target are long enough. However, there are still many unsolved issues with regard to the hole-boring RPA. For instance, it is still hard to control the intrinsic oscillation of the accelerating field [34,35], which may deteriorate the quality of the accelerated ion beam or even terminate the acceleration.

In this paper, we present an overview of the hole-boring RPA studies in theory and simulation. First, we will show the underlying physics of the hole-boring RPA. Then we will discuss the schemes proposed recently improving the quality of the accelerated ion beam in the hole-boring RPA in detail. In addition, we will propose an integrated scheme for the efficient high-quality hole-boring RPA under the laser and target conditions available soon. Finally we will present a summary and further discussions.

2. Mechanism of hole-boring radiation pressure acceleration

The mechanism of the hole-boring RPA can be explained by a 1D quasi-stationary laser piston model [35], which is verified by the particle-in-cell (PIC) simulation as shown in Fig. 1. At first, the ponderomotive force of a laser pulse (black curve) will push electrons (green curve) forward from ions. Then a strong longitudinal electric field (red curve) will be formed in the charge-separation layer between the electrons and the ions. Finally, the ions (blue curve) can be accelerated by this charge-separation field.

For simplicity, we first analyze the hole-boring RPA in the interaction of a CP laser pulse of a constant intensity I with a uniform cold plasma. In this case, a quasi-constant hole-boring velocity (the velocity of the laser-plasma interface) v_b can be expected. In the boosted frame moving with the laser-plasma interface, the radiation pressure delivered by the laser pulse to the laser-plasma surface can be estimated as [34].

$$P_L = \frac{2I}{c}\frac{1 - v_b/c}{1 + v_b/c}, \tag{1}$$

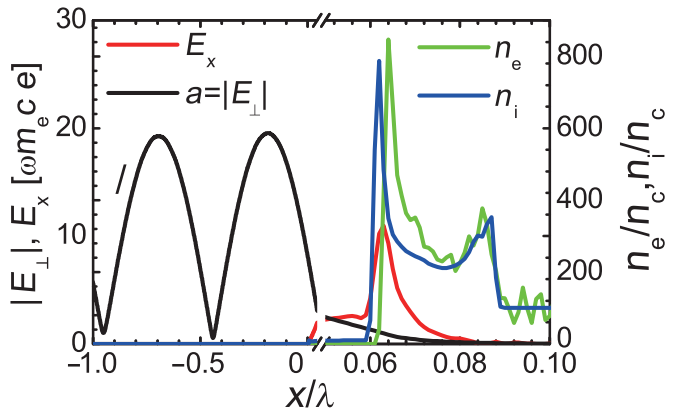

Fig. 1. Density distributions of the electrons (green curve) and the ions (blue curve) at $t = 5T_0$ obtained from a PIC simulation of a CP laser pulse interaction with a thick solid plasma, where T_0 is the laser wave period. The charge separation is indicated by the separated peaks of the electron and the ion densities. In the charge-separation layer, a very strong longitudinal electric field (red curve) is aroused, which plays a direct role in the acceleration of the ions. In this case, the laser pulse is nearly completely reflected, and the amplitude of the transversal electric field (black curve) shows that a standing wave is formed by the superposition of the reflected and incident pulses. In the simulation, the laser pulse has a trapezoidal temporal profile ($5T_0$ rise $+100T_0$ plateau $+5T_0$ fall), the peak intensity $I_0 = 2.74 \times 10^{20}$ W/cm^2 (the normalized vector potential $a \equiv |e\boldsymbol{E}/\omega m_e c| = 10$). The plasma, composed by the electrons and the protons, has an initially uniform electron number density $n_e = 100n_c$. The laser pulse is incident from the left side into the plasma. For reference, the laser pulse is assumed to arrive at the left boundary of the plasma ($x = 0$) at $t = 0$.

where the relativistic Doppler shift is taken into account and a perfect laser reflection is assumed. Meanwhile, in this boosted frame, the ions will move towards the laser-plasma interface at the speed of $-v_b$ and be reflected away. Assuming the reflection is elastic, the pressure delivered by the ions to the laser-plasma surface can be estimated as

$$P_i = 2\gamma_b^2 v_b^2 \sum_i m_i n_i, \tag{2}$$

where $\gamma = (1 - v_b^2/c^2)^{-1/2}$, the sum of $m_i n_i$ is over all ion species, and m_i and n_i are the mass and the number density of the i-th ion species, respectively.

According to the conservation of momentum in the boosted frame ($P_L = P_i$), one can get the following equation

$$(\Xi - 1)\beta_b^2 - 2\Xi\beta_b + \Xi = 0, \tag{3}$$

where $\beta_b = v_b/c$, and

$$\Xi = \frac{I}{\rho c^3} = \frac{a^2 m_e n_c}{\sum_i m_i n_i} \tag{4}$$

is the so-called pistoning parameter, ρ is the mass density of the plasma, and $n_c = m_e\varepsilon_0\omega^2/e^2$ is the critical density. Here $a \equiv |e\boldsymbol{E}/\omega m_e c|$ is the normalized vector potential of the laser pulse, for a CP laser pulse one has $a = (I/m_e n_c c^3)^{1/2} = (I\lambda^2/2.74 \times 10^{18}\ \mathrm{W \cdot cm^{-2} \cdot \mu m^2})^{1/2}$. Solving Eq. (3), one can easily get the hole-boring velocity v_b as

$$\frac{v_b}{c} = \beta_b = \frac{\sqrt{\Xi}}{1 + \sqrt{\Xi}}. \tag{5}$$

Consequently, the ion longitudinal momentum $p_{i,x}$ and the ion energy ε_i in the lab frame can be written as

$$\frac{p_{i,x}}{m_i c} = \frac{2\sqrt{\Xi}(1 + \sqrt{\Xi})}{1 + 2\sqrt{\Xi}}, \tag{6}$$

$$\frac{\varepsilon_i}{m_i c^2} = \frac{2\Xi}{1 + 2\sqrt{\Xi}}. \tag{7}$$

The energy conversion efficiency χ_i from the laser to the ions can also be calculated as

$$\chi_i = \frac{2\sqrt{\Xi}}{1 + 2\sqrt{\Xi}}. \tag{8}$$

It is worth pointing out that a relatively dense target ($n_e \geq \gamma n_c$) has been assumed in the above analysis. If the target density is relatively low ($n_e < \gamma n_c$), the effect of the relativistic transparency may become not negligible. Then the intrinsic oscillation of the accelerating field will become very strong and the accelerated ions will have a large energy spread, which will be discussed in detail below.

To verify the above theoretical analysis, the time evolution of the ion density distribution n_i in the interaction of a CP laser pulse with a thick solid plasma is displayed in Fig. 2(a). Except in the rising stage of the laser pulse, a clear boundary between the plasma and the vacuum appears. The slope of this boundary implies a nearly constant forward velocity ~0.023 c, which is in good quantitative agreement with the hole-boring velocity v_b~0.0228 estimated by theoretical Eq. (5). A very

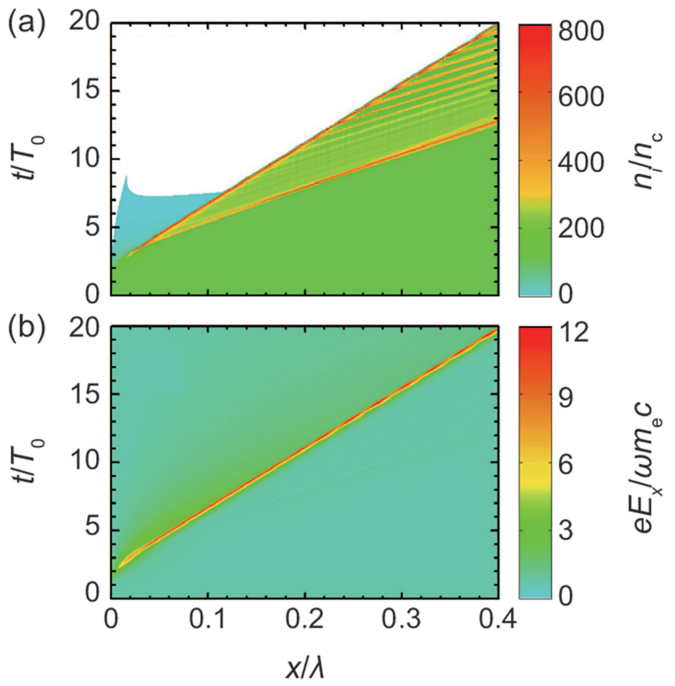

Fig. 2. Time evolution of the proton density distribution n_i and the longitudinal electric field E_x in the interaction of a CP laser pulse with a thick solid plasma. The parameters of the laser pulse and the target are the same as those in Fig. 1.

strong charge-separation field for ion acceleration is aroused at around the plasma-vacuum boundary as illuminated by the time evolution of the longitudinal electric field E_x in Fig. 2(b).

However, it is worth noting that a row of stripes appear in Fig. 2(a) sketches the contours of the high ion density regions. Further, these stripes all begin from the plasma-vacuum boundary. This indicates that the ions of these stripes are reflected and accelerated by the charge-separation electric field at the plasma-vacuum boundary. More importantly, these accelerated ions will move in bunches rather than as a constant current when they escape the charge-separation layer. This can be attributed to that the laser pulse does not act as an ideal piston [34]. The time interval among these ion bunches is inversely proportional to the ion plasma frequency [35]. Accompanied by the bunches of the reflected ions, E_x in Fig. 2(b) also oscillates slightly. This is because E_x is related to the charge number in the charge separation layer by the Possion equation, and the latter will fluctuate in time when the accelerated ions leave the layer in bunches [48].

Since the accelerated ions escape in bunches from the charge-separation layer, the ribcage-like structure appears in the ion distribution in the p_x–x phase space as shown in Fig. 3. Such a structure has been reported frequently in the previous simulations [49], and is considered as a representative phenomenon of the hole-boring RPA [34,35]. Fig. 3 also illuminates that the longitudinal momenta of the accelerated ions are distributed around $p_{i,x} \simeq 0.046\ m_i c$ as predicted by Eq. (6). The spread in the momenta can be attributed to the oscillation in the longitudinal electric field for the acceleration.

The time oscillation in the peak of the longitudinal electric field E_x,max is more clearly evidenced in Fig. 4. In Fig. 4(a), the time evolutions of the peaks of the longitudinal electric fields E_x,max are compared at different laser intensities for a given target. While the time evolutions of E_x,max in the interaction of a given laser pulse ($a = 100$) with thick targets of different densities are compared in Fig. 4(b). Although the longitudinal electric field becomes stronger with the increasing of the laser intensity, the oscillation of this field

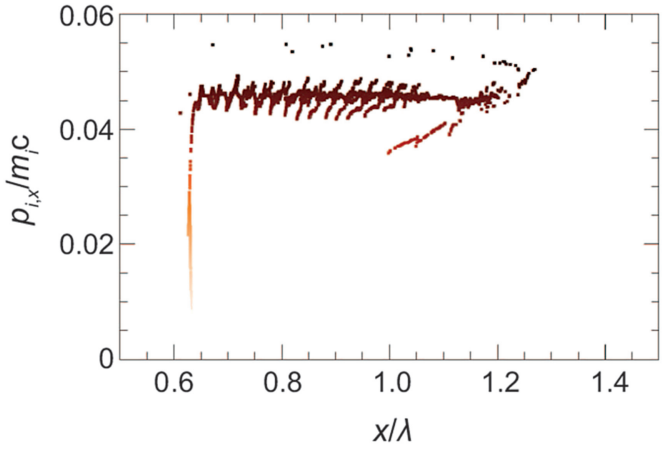

Fig. 3. Distribution of the accelerated ions in the p_x–x phase space at $t = 30T_0$ obtained from the PIC simulation of a CP laser pulse interaction with a thick solid plasma. The parameters of the laser pulse and the target are the same as those in Fig. 1.

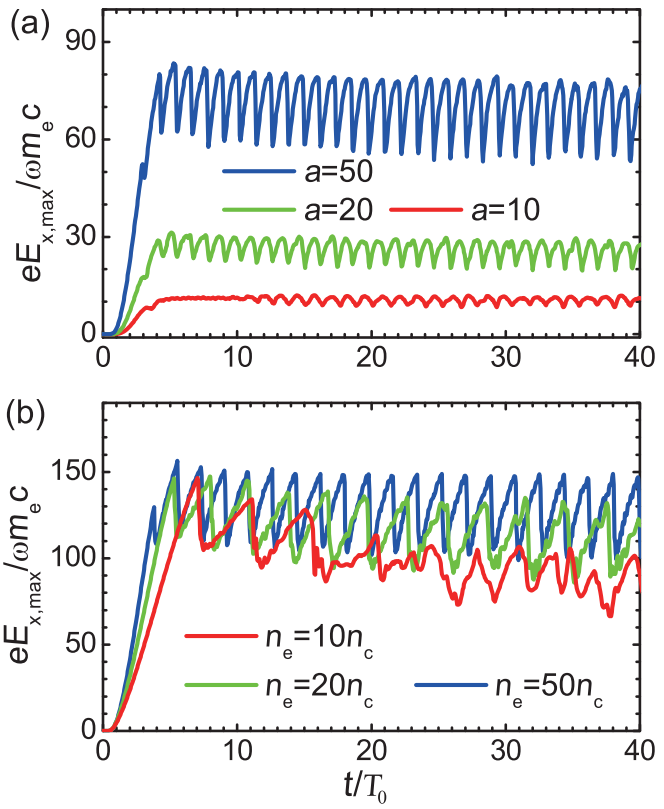

Fig. 4. Time evolutions of the peaks of the longitudinal electric fields E_x,max in the interactions of (a) a given thick solid plasma ($n_e = 100n_c$) with CP laser pulses at some different intensities $a = 10$, 20 and 50; (b) a given CP lase pulse ($a = 100$) with thick targets of different densities $n_e/n_c = 10$, 20, and 50. Other parameters of the laser pulse and the target are the same as those in Fig. 1.

peak also becomes more violent in Fig. 4(a). The oscillation of the peak of the accelerating field also becomes more violent with the decreasing of the target density as shown in Fig. 4(b). In most cases, the peak of the electric field oscillates in a "saw-tooth" form, resulting in the fine ribcage-like structure presented in the ion distribution in the p_x–x phase space as shown in Fig. 3. In the case of a high laser intensity ($a = 100$) with a low target density ($n_e = 10n_c$), however, there is nearly no regularity in the time evolution of the electric field. Here the relativistic transparency [50] plays an important role, so one enters an incomplete hole-boring RPA regime [51]. It was shown that the energy of accelerated ions can be significantly increased in this incomplete hole-boring RPA. However, the quality of being quasi-monoenergetic is nearly lost due to the strong oscillation in the accelerating field in this regime. By a series of 1D numerical simulations, it is found that the boundary density between the classic hole-boring RPA and the incomplete hole-boring RPA can be estimated as [51].

$$n_b = 0.618\left(1 + 2a^2\right)^{0.314} n_c, \tag{9}$$

for plasmas composed by protons and electrons.

According to Eqs. (5) and (7), the energy of the accelerated ions in the hole-boring RPA will be enhanced by the increase of the laser intensity or the decrease of the target density. This scaling law is verified by PIC simulations as shown in Fig. 5.

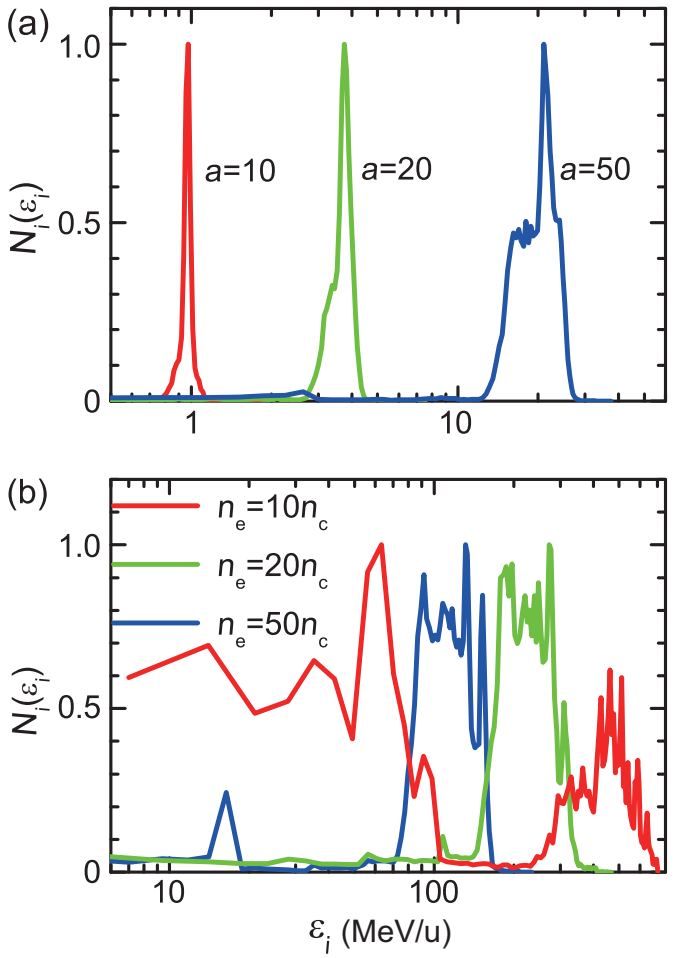

Fig. 5. Ion energy spectra at $t = 50T_0$ in the interactions of (a) a given thick solid plasma ($n_e = 100n_c$) with CP laser pulses at some different intensities $a = 10$, 20 and 50; (b) a given CP lase pulse ($a = 100$) with thick targets of different densities $n_e/n_c = 10$, 20, and 50. The logarithmic coordinate is used for the ion energy. The parameters of the laser pulse and the target are the same as those in Fig. 1.

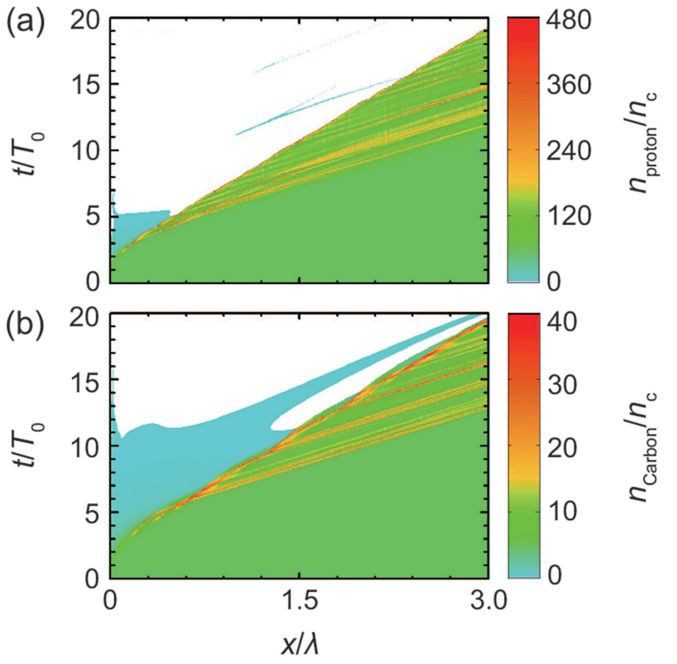

Fig. 6. Time evolutions of (a) proton and (b) C^{6+} ion density distributions in the interaction of a CP laser pulse ($a = 85$) with a composite CH target. The CH target is composed of carbon and hydrogen in 1:1 mass ratio, and has the number densities $n_C^{6+} = 5n_c$, $n_H^+ = 60n_c$, and $n_e = 90n_c$ for C^{6+} ions, protons, and electrons, respectively. Other parameters of the laser pulse and the target are the same as those in Fig. 1.

However, it is worth emphasizing that the energy spread also becomes larger with the increasing laser intensity or the decreasing target density due to the enhanced oscillation in the accelerating field as shown in Fig. 4. In other words, in the hole-boring RPA, the ion energy is usually enhanced at the cost of the quality of the ion beam. To date, it still remains a critical issue to enhance both the energy and the quality of the accelerated ion beam in the hole-boring RPA, or generally speaking in the laser-driven ion acceleration.

3. Schemes to improve ion beam quality

In the last decade, a lot of efforts have been made to control the acceleration stability and to improve the quality of generated beams in laser-driven ion accelerations. In the particular realm of the light-sail RPA, the shape, composition, and structure of foil targets as well as the contrast and profile of laser pulses have been systematically optimized for generating quasi-monoenergetic ion beams [29,30,52–54]. In contrast to the light-sail RPA, the hole-boring RPA don't have so many stringent requirements in laser or target conditions, such as an ultrahigh laser contrast [55]. However, it is found that the beam energy spectrum and divergence in the hole-boring RPA also strongly rely on the laser and target parameters [47]. In addition, circularly polarized laser pulses are commonly employed in the hole-boring RPA to suppress the generation of hot electrons that results in the exponential ion spectra by TNSA.

In this section, we will further discuss some schemes proposed recently to enhance the ion beam quality in the hole-boring RPA. First, it is found that the oscillation in the accelerating field can be greatly suppressed by using two-ion-species targets, which plays an important role in reducing the energy spread of the accelerated ions. Secondly, the matching condition between laser intensity profile and target density profile is formulated for the efficient generation of high-quality ion beams by the hole-boring RPA. This matching condition can be applied in tailoring the laser temporal profile for achieving a steady hole-boring in an inhomogeneous target, or conversely in modulating the target density distribution in accordance with a Gaussian laser pulse. Finally, based on the available laser technology and target fabrication techniques, an integrated scheme will be introduced for the efficient high-quality hole-boring RPA.

3.1. Two-ion-species target design

Many numerical simulations demonstrate that composite targets with two ion species play a positive role in stabilizing the acceleration process and reducing the ion energy spread in

the light-sail RPA [30,56] or the TNSA [57]. In the hole-boring RPA, the two-ion-species targets have a similar effect, although the underlying physics seems more complicated [58].

As shown in the above section, the longitudinal accelerating field in the hole-boring RPA inherently oscillates with the discrete reflection of ions in bunches from the charge-separation layer. And this intrinsic oscillation in the accelerating field results in the broad distribution of accelerated ions in energy. Therefore, the dynamics of accelerated ions is the key to understand the effect of two-ion-species targets upon the ion energy spread in the hole-boring RPA.

The time evolutions of proton and C^{6+} ion density distributions in the hole-boring ion acceleration using a composite CH target are displayed in Fig. 6(a) and (b), respectively. As predicted, the accelerated ions move in bunches when they escape the charge-separation layer. However, the protons and C^{6+} ions are divided into respective bunches since they have different charge-to-mass ratios. Further, more chaos appear and the time intervals between these ion bunches seem no longer constant in both Fig. 6(a) and (b), which may be due to the interference between the proton bunches and C^{6+} ion bunches. As a result, the protons and C^{6+} ions accelerated from the composite CH target are allocated into a larger number of bunches, while each ion bunch has a lower charge.

Thanks to these smaller bunches of the accelerated ions, one can expect that the charge density oscillation in the charge-separation layer will become weaker, so does the oscillation in the charge-separation electric field. The time evolution of the amplitudes of the accelerating field in the above composite CH target, a pure hydrogen target, and a pure carbon target are compared in Fig. 7. Since the mass density in these three targets are set to be equal, the peaks of the longitudinal electric field are almost equal on the average. However, the relative oscillations in the field peaks ΔE_x,max/E_x,max are roughly 30% and 10% for the pure hydrogen (or carbon) targets and the composite CH target, respectively. It is clearly verified that a smoother accelerating field can be achieved by using a composite target in the hole-boring RPA.

Since the oscillation in the accelerating field has been effectively controlled in a composite target, the energy spread of the accelerated ions in the hole-boring RPA is naturally reduced as shown in Fig. 8.

However, it is important to emphasize that the underlying mechanism for the energy spread reducing by using a composite target in the hole-boring RPA is essentially different from those in the TNSA or the light-sail. In the TNSA (light-sail RPA), the protons as the lightest ions are more easily to be accelerated by the charge-separation field in the sheath (double layer), while the heavier ions lag behind. The laggard heavier ions will provide a Coulomb repulsion which could accelerate the protons further. Therefore, the protons can be accelerated to a higher energy [30,56,57]. Further, the heavier ions can shield the protons from the transverse instabilities to some extent. Therefore, the accelerating field upon the protons will become more stable. As a result, a quasimonoenergetic proton beam could be generated [30,56,57]. However, a large fraction of laser energy is also deposited into the heavier ions. These heavier ions usually have a larger energy spread that may discourage their application. In the hole-boring RPA, however, protons and heavier ions (such as C^{6+} ions) in a composite target can be accelerated synchronously. Therefore, their spectra are very similar. Fig. 8 displays that both spectra have peak energies at around 58 MeV/u and FWHM spreads $\Delta E/E \simeq 20\%$.

3.2. Matching of laser intensity and target density profiles

It is worth pointing out that the laser intensities are all assumed to be constant and the target densities are all assumed to be uniform in the above analyses and simulations. However, inhomogeneous plasmas are present everywhere in laser-plasma interactions. In particular, the pre-compressed fuel target for ICF or the pre-plasma produced by the pre-pulse usually have exponential density profiles [40,59]. On the

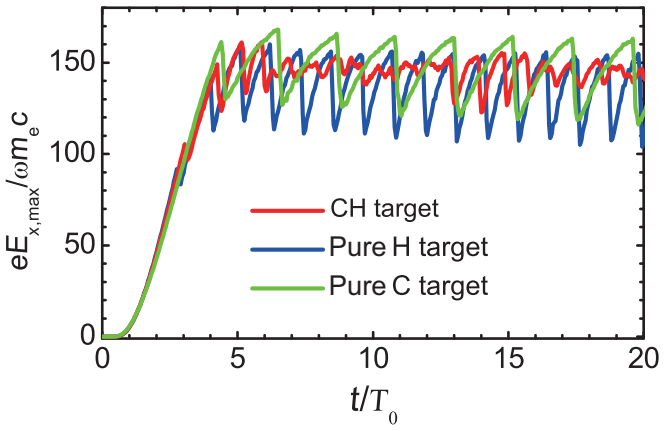

Fig. 7. Time evolution of the amplitudes of the accelerating field E_x,max in the interactions of a CP laser pulse with three different targets: the composite CH target as used in Fig. 6, a pure hydrogen target with $n_e = 10n_H = 120n_c$, and a pure carbon target with $n_e = 5n_H = 60n_c$. Noting that these three targets have the same mass density. Other parameters of the laser pulse and the target are the same as those in Fig. 6.

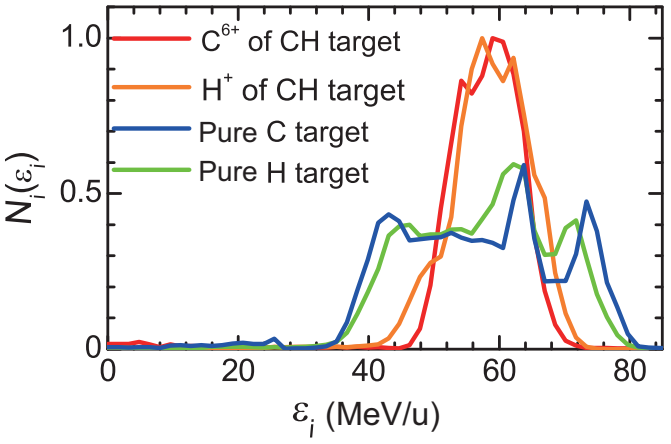

Fig. 8. Ion energy spectra at $t = 50T_0$ in the interactions of a CP laser pulse ($a = 85$) with three different targets: a composite CH target, a pure hydrogen target, and a pure carbon target. The applied laser pulse and target are the same as those in Fig. 7.

other hand, laser pulses often have Gaussian intensity profiles in both temporal and spatial domains. In these cases, the match between the laser intensity profile and the target density distribution is critical for the efficient generation of high-quality ion beams in the hole-boring RPA.

Now we first consider the tailoring of the laser pulse for achieving a steady hole-boring RPA in an inhomogeneous target. For the sake of simplicity, a semi-infinite target is assumed in the half-space $x \geq 0$ and a laser pulse is incident from the left side onto the target. The density profile of the target is $\rho(x)$ and the temporal intensity profile of the pulse is $I(t)$. Eqs. (5) and (7) suggest that a time-independent hole-boring velocity v_b can be achieved in an inhomogeneous plasma if the parameter Ξ_0 keeps constant. Due to this time-independent v_b, the ions can be accelerated to the same energy roughly. Consequently, a monoenergetic ion beam can be produced. Assuming a time-independent $v_b = c\sqrt{\Xi_0}/(1+\sqrt{\Xi_0})$, the time t_s when the slice at the t' interval of the laser pulse arrives at the instantaneous laser-plasma interface can be obtained from the relation $ct_s = ct' + v_b t_s$. Thus the instantaneous position of the laser-plasma interface is given by

$$x' = v_b t_s = c\sqrt{\Xi_0}t'. \tag{10}$$

Combining the above equation with the definition of Ξ gives the matching condition between the laser intensity profile and the target density profile for the generating of quasi-monoenergetic ions as [40].

$$I(t) = \rho(x)c^3\Xi_0 = \rho\left(c\sqrt{\Xi_0}t\right)c^3\Xi_0. \tag{11}$$

For an exponential density profile $\rho(x) = \rho_0\exp(x/L)$ with a scale length L [59], the above matching condition results in a temporal intensity profile for the tailored laser pulse as $I(t) = I_0\exp(t/T_s)$ with the beginning intensity $I_0 = \rho_0 c^3\Xi_0$ and the time scale length $T_s = L/c\sqrt{\Xi_0}$. Correspondingly, the normalized vector potential should have the following profile

$$a(t) = a_0\exp(t/2T_s), \tag{12}$$

where $a_0 = (\Xi_0 \sum m_i n_{i0}/m_e n_c)^{1/2}$, ρ_0 and n_{i0} are respectively the mass density and the i-th ion number density at the left boundary, and Z is the ionic charge state.

Further, the match between the target with $\rho(x) = \rho_0\exp(x/L)$ and the laser pulse with a tailored temporal profile given by Eq. (12) is not so sensitive to the pre-pulse or the pre-plasma, which may greatly relax the contrast requirement in the experimental realization. Regardless of the beginning intensity I_0 of the laser pulse or the plasma boundary density ρ_0, theoretical analysis and simulations [40] have demonstrated that a convergent hole-boring velocity can be achieved if the main pulse and the plasma are long enough. And the convergent hole-boring velocity $v_b(t\to\infty) = cL/(cT_s + L)$ depends only on the pulse time scale length T_s and the plasma density scale length L.

As shown in Fig. 9, a nearly time-independent hole-boring velocity has been verified, where the temporal intensity profile of the laser pulse is tailored according to the density profile of an inhomogeneous plasma. In the simulation, the inhomogeneous plasma is a composite target that composed of carbon and hydrogen in 1:1 mass ratio. The target has an exponential electron density profile $n_e(x) = 20n_c\exp(x/20\lambda)$ in the ramp region $0 \leq x \leq 50\lambda$ and then remains uniform in the region $x \geq 50\lambda$. Eq. (12) suggests that a tailored laser pulse $a(t) = a_0\exp(t/2T_s)$ with $a_0 = 26.87$ and $T_s = 174.7T_0$ can produce a nearly time-independent hole-boring velocity $v_b = 0.1027c$ (i.e., $\Xi_0 = 0.0131$). Simulation result using such a tailored pulse has been displayed in Figs. 9–11, where the laser pulse is terminated at 400 laser wave cycles. As shown in Fig. 9, a nearly time-independent $v_b \simeq 0.103c$ has been verified by the simulation.

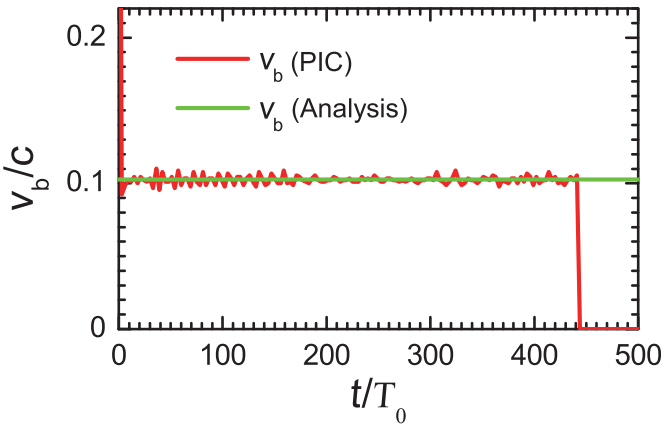

Fig. 9. The time evolution of the propagation velocity of the laser-plasma interface, where the temporal intensity profile of the laser pulse is tailored according to the density profile of an inhomogeneous plasma. The simulation result (red curve) is compared with the hole-boring velocity by the analytic prediction (green curve). In this case, the hole-boring velocity is equivalent to the propagation velocity of the laser front. The position of the laser front in the simulation is defined as the point where the local incident laser intensity is equal to $I_0/4$. The laser and target parameters are given in the text.

Since the front propagation velocity of the tailored laser pulse is nearly constant, the ions of the inhomogeneous plasma

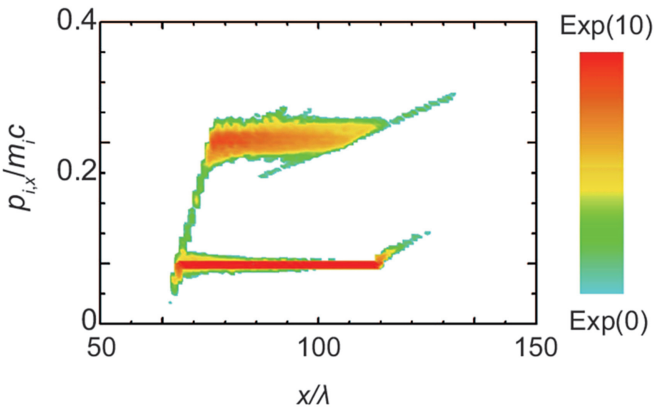

Fig. 10. Ion momentum distribution at $t = 500T_0$ after the interaction of a tailored laser pulse with an inhomogeneous plasma. Here we don't separately show the distributions for protons and carbon ions, since they are similar to that of total ions. A time-independent mean momentum is evident. The laser and target parameters are given in the text.

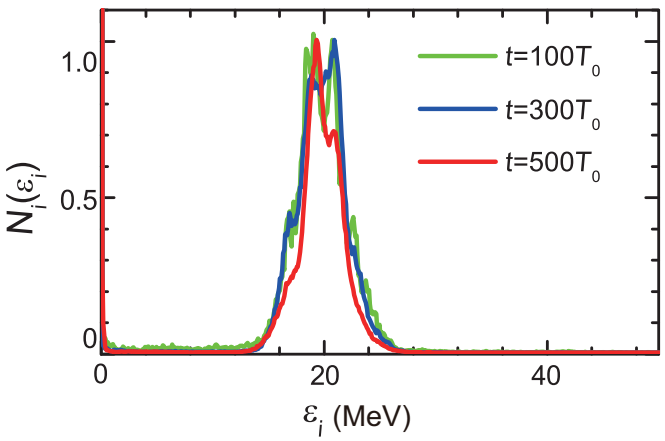

Fig. 11. Ion energy spectra at different moments $t = 100$, 300, and 500 T_0 in the interaction of a tailored laser pulse with an inhomogeneous plasma. Here we don't separately show the spectra for protons and carbon ions, since they are similar to that of total ions. The laser and target parameters are given in the text.

will be reflected by a steady moving laser-plasma interface. Consequently, the accelerated ions have a time-independent mean momentum $p_{i,x} \simeq 0.2 m_i c$ as shown in Fig. 10. This time-independent mean momentum is also in good agreement with the analytic prediction by Eq. (6).

Thanks to the nearly time-independent hole-boring velocity, the accelerated ions will naturally have a narrow energy spread. More importantly, such a narrow energy spread can be well preserved in the whole interaction of the tailored pulse with the inhomogeneous plasma. As shown in Fig. 11, the energy spectra at three different moments $t = 100$, 300, and $500T_0$ have a self-similar shape with an energy spread about 20%. Since the good monoenergetic quality of accelerated ions is time-independent, this scheme is particularly suitable for the generating of a high-fluence quasi-monoenergetic ion beam using tailored long-pulsed lasers.

Recent simulations show that it is very attractive to realize the *in-situ* hole-boring fast ion ignition by temporally tailored laser pulses [40]. In the hole-boring process of an ultraintense laser pulse into a pre-compressed deuterium-tritium (DT) target, a large number of fast ions will be generated by the hole-boring RPA. In the so-called *in-situ* fast ion ignition [14], it is proposed that the DT target be ignited directly by the hole-boring accelerated ions. This *in-situ* hole-boring fast ion ignition scheme does not require a separate target for the ion acceleration, so it is particularly suitable for the high repetition rate operation. In addition, the requirements for the beam quality can be significantly relaxed due to the short distance between the acceleration zone and the ignition core [60]. However, the pre-compressed DT target is highly inhomogeneous, so a tailored laser pulse is critically required to achieve the efficient high-quality hole-boring RPA in this scheme. Simulations indicate that the required laser energy for the acceleration laser pulse in the *in-situ* hole-boring fast ion ignition can be reduced from a few hundred kJ to about 65 kJ by using tailored laser pulses [40].

However, it is still extremely difficult to precisely shape the temporal intensity profile of an ultrashort (~ ps) laser pulse by the current laser technology. So we propose an alternative route to the efficient high-quality hole-boring RPA, namely, modulating the target density in accordance with the Gaussian laser pulse. By virtue of the pulsed laser deposition technique [61] or the layer-by-layer nanoarchitectonics [62,63], it may be easier to tailor the density profile of a solid target than the intensity profile of a rapidly changing laser pulse.

If the laser pulse has a Gaussian temporal profile $I(t) = I_0 \exp(-2.77t^2/\tau_L^2)$, then the matching condition (11) specializes the density profile of the modulated target as

$$\rho(x) = \rho_0 \exp\left(-2.77x^2/L_x^2\right), \tag{13}$$

where I_0 and τ_L are the laser pulse peak intensity and FWHM duration, respectively; $\rho_0 = I_0/c^3\Xi_0$ and $L_x = c\sqrt{\Xi_0}\tau_L$ are the plasma peak density and FWHM dimension in x direction, respectively.

In Fig. 12, the ion energy spectra obtained in the laser interactions with a uniform target and a density-modulated target are compared. The laser intensity profile is given as $a(t) = a_0 \exp[-2.77(t/\tau_L)^2/2]$ with $a_0 = 100$ and $\tau_L = 30T_0$. The uniform target is composed of carbon and hydrogen in 1:2

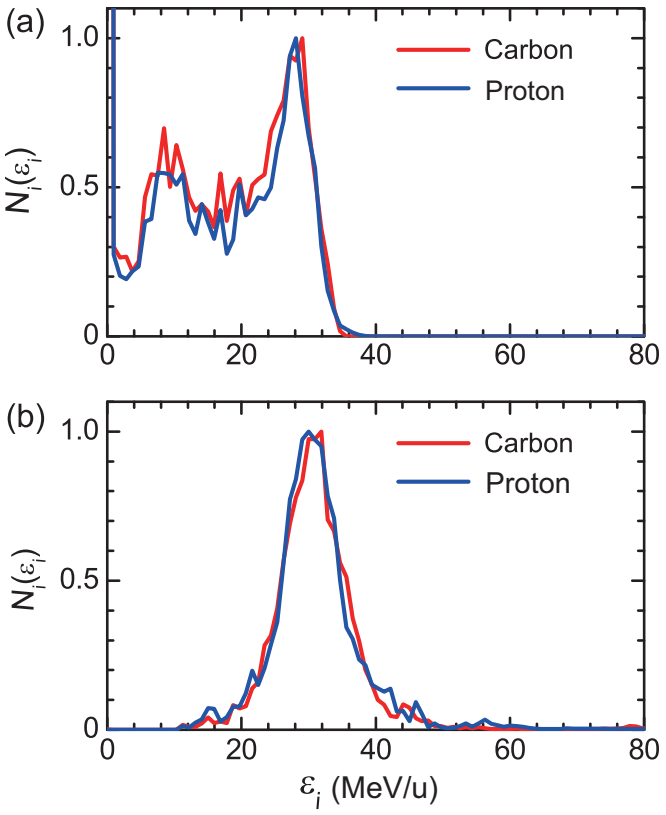

Fig. 12. Proton (blue curves) and C^{6+} ion (red curves) energy spectra at $t = 50T_0$ after the interactions of a Gaussian laser pulse with (a) a uniform CH target and (b) a density-modulated CH target, respectively. For reference, the laser pulse peak is assumed to arrive at the left boundary of the uniform target ($x = 0$) or the center of the density-modulated target ($x = 0$) at $t = 0$. And for convenience the modulated target is cut off at $\rho = \rho_0/10$ in the simulation.

number ratio, and the number densities are $n_C^{6+} = 18n_c$ and $n_H = 36n_c$ for C^{6+} ions and the protons, respectively. The density modulated target is also composed of carbon and hydrogen in 1:2 number ratio, but the number density profiles are defined as $n_C^{6+}(x) = 18n_c\exp[-2.77(x/L_x)^2]$ and $n_H = 36n_c\exp[-2.77(x/L_x)^2]$ for C^{6+} ions and protons, respectively. Here, $L_x = c\Xi_0\tau_L = 4.41\lambda$ with $\Xi_0 = 0.147$. According to Eq. (13), the applied Gaussian laser pulse will result in a nearly constant hole-boring velocity $v_b = c\Xi_0/(1+\Xi_0) \simeq 0.128c$ in the density-modulated target and generate quasi-monoenergetic ions at $E_i \simeq 31$ MeV/u. The generation of a quasi-monoenergetic ion beam at ~30 MeV from this density-modulated target is confirmed in the PIC simulation as shown in Fig. 12(b). While a broader energy spectrum is produced with the uniform target in Fig. 12(a).

3.3. An integrated scheme

In the above section, we have discussed about the modulating of the longitudinal density profile of a target to couple with a temporally Gaussian laser pulse. Theoretically, we can also modulate the transverse density profile of a target to couple with a spatially Gaussian laser pulse for the efficient high-quality hole-boring RPA in multi-dimensional cases. However, this requires to aim the laser pulse precisely at the center of the density-modulated target, which is still a big challenge to current laser technology [54]. If there is a displacement of the target off the axis of the laser pulse, the quality of the accelerated ion beam, especially its collimation, will become much worse than expected as shown in Figs. 13(a), 14(a) and 15.

Therefore, based on the comprehensive consideration of the above factors, we suggest the following integrated scheme for achieving the efficient high-quality hole-boring RPA in the experiments: (a) using composite targets with at least two ion species; (b) modulating the target longitudinal density profile; and (c) tailoring the laser transverse intensity profile. For simplicity, we suggest a super-Gaussian transverse profile for the laser pulse.

We display the target dynamics in the hole-boring PRA using this integrated scheme in Fig. 13(b). It is illustrated that the middle part of the partially density-modulated target irradiated by the laser pusle can be efficiently accelerated exactly along the axis of the laser pulse. However, a fully density-modulated target will be driven away the axis further and further if there is an initial displacement of the target off the axis of the laser pulse. Therefore, the accelerated ions by the integrated scheme using a super-Gaussian laser pulse and a partially density-modulated target is well collimated along the axis of the laser pulse as shown in Fig. 14(b). While the ions accelerated from a fully density-modulated target by a Gaussian laser pulse may have large deviation angles ~15° as shown in Fig. 14(a).

The ion energy spectrum obtained in the hole-boring PRA using the integrated scheme is displayed in Fig. 15, which shows a clear peak at around 33 MeV/u. This peak energy is in good agreement with the predication by Eq. (7) with

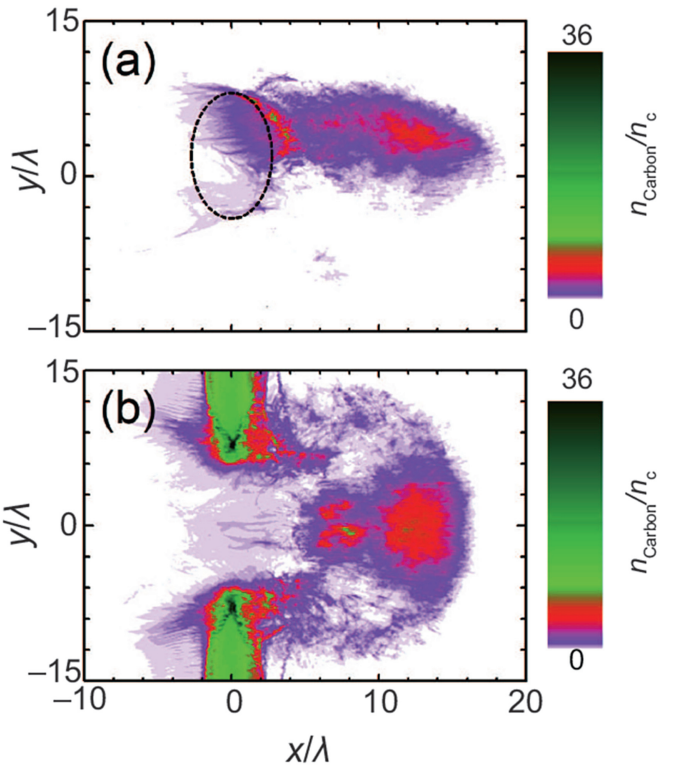

Fig. 13. Carbon ion density distributions at $t = 50T_0$ after the interactions of (a) a Gaussian laser pulse with a target whose density profile is fully modulated in both the longitudinal and transversal directions with a displacement of 2λ between the laser pulse and the target axes; (b) a super-Gaussian laser pulse with a target whose density profile is partially modulated only in the longitudinal direction. In (a), the laser pulse has a temporally and spatially Gaussian intensity profile $a(t,r) = a_0(-2.77t^2/\tau_L^2)\exp[-r^2/\sigma^2]$ with $a_0 = 85$, $\tau_L = 20T_0$, and $\sigma = 4\lambda$, the fully modulated target has an electron number density profile $n_e(x,y) = 100n_c\exp(-2.77x^2/L_x^2)\exp[-(y-2\lambda)^2/\sigma^2]$ with $L_x = c\Xi_0\tau_L = 3\lambda$. In (b), the laser pulse has a spatially super-Gaussian and temporally Gaussian intensity profile $a(t,r) = a_0(-2.77t^2/\tau_L^2)\exp[-r^5/\sigma^5]$ with $a_0 = 85$, $\tau_L = 20T_0$, and $\sigma = 4\lambda$, the target density is modulated only in the longitudinal direction as $n_e(x,y) = 100n_c\exp(-2.77x^2/L_x^2)$ with $L_x = 3\lambda$. For convenience, the modulated targets are cut off at $n_e = 10n_c$ in both (a) and (b). And they are composed of carbon and hydrogen in 1:2 number ratio, so the peak ion number densities are $n_C^{6+} = 12.5n_c$ and $n_H = 25n_c$ for C^{6+} ions and protons, respectively. The dashed ellipse in (a) demarcates the initial boundary of the density-modulated target. For reference, the peaks of both laser pulses are assumed to arrive at $x = 0$ at $t = 0$. The density distributions of the protons are similar to those of C^{6+} ions and thus are omitted here.

$\Xi_0 = 0.15$. In the scheme using a Gaussian laser pulse with a fully density-modulated target, however, the quality of being quasi-monoenergetic will be lost for the accelerated ions if there is an off-axis displacement between the laser pulse and the target. On the consideration of the laser-target alignment, therefore, it is more reliable to achieve the high-quality hole-boring RPA by the integrated scheme, which tailors the target longitudinal density profile together with the laser transverse intensity profile.

4. Discussion and summary

Compared with the light-sail RPA, the energy scaling law of the hole-boring RPA may not allow it to accelerate the ions

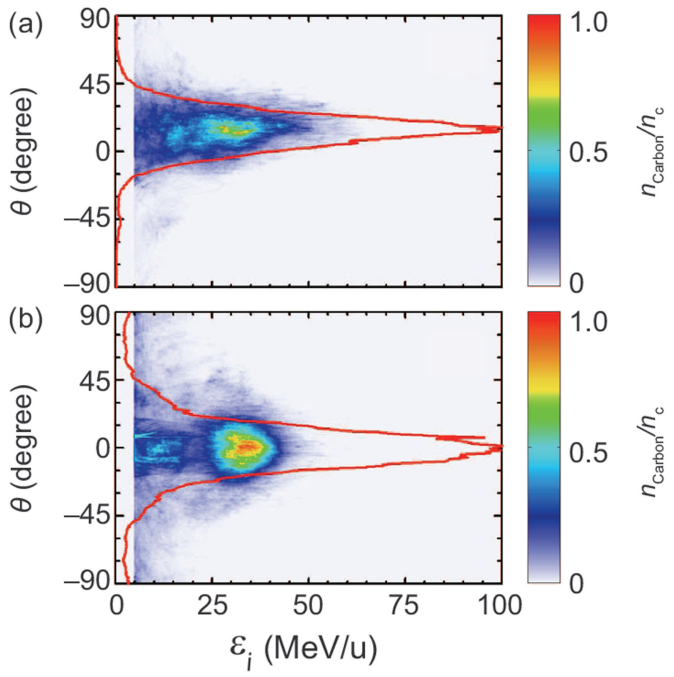

Fig. 14. Carbon ion energy-angle distributions at $t = 50T_0$ after the interactions of (a) a Gaussian laser pulse with a fully density-modulated target; (b) a super-Gaussian laser pulse with a partially density-modulated target. The parameters of the laser pulse and the target are the same as those in Fig. 13.

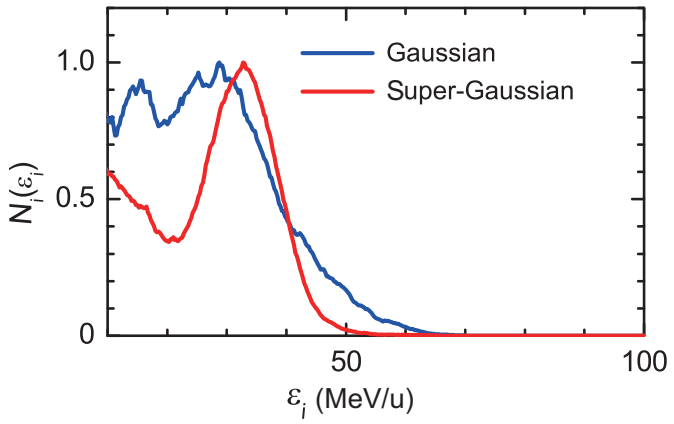

Fig. 15. Carbon ion energy spectra at $t = 50T_0$ after the interactions of a Gaussian laser pulse with a fully density-modulated target (the blue curve) and a super-Gaussian laser pulse with a partially density-modulated target (the red curve). The parameters of the laser pulse and the target are the same as those in Fig. 13.

up to the level of GeV/u [55]. However, the advantages of the hole-boring RPA lie in that the required laser contrast is modest, and particularly the accelerated ion number can be extremely large. The high-fluence quasi-monoenergetic plasma block produced in the hole-boring RPA using the improved integrated scheme is particularly interesting for fast ignition of ICF, or more generally for the creation of high energy density conditions due to the presence of the Bragg peak for mono-energetic ion beams [10,38,39,41,42]. Further, the unique short duration (~100 fs) of the produced ion beams is especially suitable for isochoric heating of solid-density matter [8,9,44,64]. In addition, this kind of high energy density plasma blocks may permit the side-on ignition of uncompressed solid target for a neutron-free ultra-clean fusion [65,66]. As in the light-sail RPA, circularly polarized high-power laser pulses are critically required in the hole-boring RPA in order to suppress the plasma heating. Although a quarter-wave plate can transfer a linearly polarized laser pulse into a circularly polarized one, its diameter would be as large as a few meters in order to avoid the laser-induced damage if the laser power is as high as 10 PW. To manufacture such a large quarter-wave plate is still an extreme challenge to the current technology. Based on an extreme Faraday effect found recently [67], one may realize a new type of magnetized plasma polarizer on the scale of a few centimeters to convert linear polarized pulses to circularly polarized ones for such high power laser pulses.

We notice that there are also a few other optimizations for the acceleration of plasma blocks by laser pulses, such as introducing a pre-target with a relatively low density in front of the main dense target [68–70]. In this case, the charge separation field in the main target can be greatly enhanced, which then enhances the energy, ion number and quality of the accelerated plasma blocks. With a pre-target or pre-plasma, however, the density modification due to the nonlinear ponderomotive force may become significant [44,71]. Further, with a pre-plasma the laser pulse could be tightly focused down to a diameter of the order of the laser wavelength due to the relativistic self-focusing [71]. In such an extreme case, the longitudinal field components of the laser pulse could also play an important role in the acceleration of particles [44,72–74].

To summarize, we first retrospected the mechanism of the hole-boring RPA, especially the physics underlying the oscillation in the accelerating field. Based on this, we discussed about the suppression of this oscillation in the accelerating field by using two-ion-species targets, and hence the reducing of the ion energy spread in the hole-boring RPA. Further, the intensity profile of the laser pulse and the density profile of the target were optimized for the hole-boring RPA. Finally, an integrated scheme was introduced for the efficient high-quality hole-boring RPA, in which the longitudinal density profile of a composite target together with the laser transverse intensity profile are shaped according to the matching condition.

Acknowledgments

This work was supported in part by the National Basic Research Program of China (Grant No. 2013CBA01504) and the National Natural Science Foundation of China (Grant Nos. 11675108, 11421064, 11405108 and 11374210). S.M. Weng and M. Chen appreciate the supports from National 1000 Youth Talent Project of China. Z.M.S acknowledges the support of a Leverhulme Trust Research Project Grant at the University of Strathclyde. Simulations have been carried out at the PI cluster of Shanghai Jiao Tong University.

Conflict of interest

The authors declare that there is no conflicts of interest.

References

[1] H. Daido, M. Nishiuchi, A.S. Pirozhkov, Review of laser-driven ion sources and their applications, Rep. Prog. Phys. 75 (2012) 056401.

[2] A. Macchi, M. Borghesi, M. Passoni, Ion acceleration by superintense laser-plasma interaction, Rev. Mod. Phys. 85 (2013) 751.

[3] S. Kawata, T. Nagashima, M. Takano, T. Izumiyama, D. Kamiyama, et al., Controllability of intense-laser ion acceleration, High Power Laser Sci. Eng. 2 (2014) e4.

[4] Y.J. Gu, Z. Zhu, X.F. Li, Q. Yu, S. Huang, et al., Stable long range proton acceleration driven by intense laser pulse with underdense plasmas, Phys. Plasmas 21 (2014) 063104.

[5] M. Borghesi, D.H. Campbell, A. Schiavi, M.G. Haines, O. Willi, et al., Electric field detection in laser-plasma interaction experiments via the proton imaging technique, Phys. Plasmas 9 (2002) 2214.

[6] S.S. Bulanov, A. Brantov, V. Yu. Bychenkov, V. Chvykov, G. Kalinchenko, et al., Accelerating protons to therapeutic energies with ultra-intense ultra-clean and ultra-short laser pulses, Med. Phys. 35 (2008) 1770.

[7] J.S. Loeffler, M. Durane, Charged particle therapy—optimization, challenges and future directions, Nat. Rev. Clin. Oncol. 10 (2013) 411.

[8] P.K. Patel, A.J. Mackinnon, M.H. Key, T.E. Cowan, M.E. Foord, et al., Isochoric heating of solid-density matter with an ultrafast proton beam, Phys. Rev. Lett. 91 (2003) 125004.

[9] N.A. Tahir, C. Deutsch, V.E. Fortov, V. Gryaznov, D.H.H. Hoffmann, et al., Proposal for the study of thermophysical properties of high-energy-density matter using current and future heavy-ion accelerator facilities at GSI Darmstadt, Phys. Rev. Lett. 95 (2005) 035001.

[10] M. Roth, T.E. Cowan, M.H. Key, S.P. Hatchett, C. Brown, et al., Fast ignition by intense laser-accelerated proton beams, Phys. Rev. Lett. 86 (2001) 436.

[11] M. Tabak, J. Hammer, M.E. Glinsky, W.L. Kruer, S.C. Wilks, et al., Ignition and high gain with ultrapowerful lasers, Phys. Plasmas 1 (1994) 1626.

[12] S. Pfalzner, An Introduction to Inertial Confinement Fusion, 1Taylor & Francis Group, New York, 2006.

[13] J.J. Honrubia, J.C. Fernández, M. Temporal, B.M. Hegelich, J. Meyer-ter-Vehn, Fast ignition of inertial fusion targets by laser-driven carbon beams, Phys. Plasmas 16 (2009) 102701.

[14] N.N. Naumova, T. Schlegel, V.T. Tikhonchuk, C. Labaune, I.V. Sokolov, et al., Hole boring in a DT pellet and fast-ion ignition with ultraintense laser pulses, Phys. Rev. Lett. 102 (2009) 025002.

[15] B.M. Hegelich, D. Jung, B.J. Albright, J.C. Fernandez, D.C. Gautier, et al., Experimental demonstration of particle energy, conversion efficiency and spectral shape required for ion-based fast ignition, Nucl. Fusion 51 (2011) 083011.

[16] S.C. Wilks, A.B. Langdon, T.E. Cowan, M. Roth, M. Singh, et al., Energetic proton generation in ultra-intense laser-solid interactions, Phys. Plasmas 8 (2001) 542.

[17] M. Passoni, L. Bertagna, A. Zani, Target normal sheath acceleration: theory, comparison with experiments and future perspectives, New J. Phys. 12 (2010) 045012.

[18] Q.L. Dong, Z.M. Sheng, M.Y. Yu, J. Zhang, Optimization of ion acceleration in the interaction of intense femtosecond laser pulses with ultrathin foils, Phys. Rev. E 68 (2003) 026408.

[19] L. Yin, B.J. Albright, B.M. Hegelich, J.C. Fernandez, GeV laser ion acceleration from ultrathin targets: the laser break-out afterburner, Laser Part. Beams 24 (2006) 291.

[20] C.A.J. Palmer, N.P. Dover, I. Pogorelsky, M. Babzien, G.I. Dudnikova, et al., Monoenergetic proton beams accelerated by a radiation pressure driven shock, Phys. Rev. Lett. 106 (2011) 014801.

[21] D. Haberberger, S. Tochitsky, F. Fiuza, C. Gong, R.A. Fonseca, et al., Collisionless shocks in laser-produced plasma generate monoenergetic high-energy proton beams, Nat. Phys. 8 (2012) 95.

[22] M. Liu, S.M. Weng, Y.T. Li, D.W. Yuan, M. Chen, et al., Collisionless electrostatic shock formation and ion acceleration in intense laser interactions with near critical density plasmas, Phys. Plasmas 23 (2016) 113103.

[23] K. Nishihara, H. Amitani, M. Murakami, S.V. Bulanov, T.Zh. Esirkepov, High energy ions generated by laser driven Coulomb explosion of cluster, Nucl. Instr. Meth. A 464 (2001) 98.

[24] M. Murakami, M. Tanaka, Generation of high-quality mega-electron volt proton beams with intense-laser-driven nanotube accelerator, Appl. Phys. Lett. 102 (2013) 163101.

[25] T. Esirkepov, M. Borghesi, S.V. Bulanov, G. Mourou, T. Tajima, Highly efficient relativistic-ion generation in the laser-piston regime, Phys. Rev. Lett. 92 (2004) 175003.

[26] A.P.L. Robinson, M. Zepf, S. Kar, R.G. Evans, C. Bellei, Radiation pressure acceleration of thin foils with circularly polarized laser pulses, New. J. Phys. 10 (2008) 013021.

[27] X.Q. Yan, C. Lin, Z.M. Sheng, Z.Y. Guo, B.C. Liu, et al., Generating high-current monoenergetic proton beams by a circularly polarized laser pulse in the phase-stable acceleration regime, Phys. Rev. Lett. 100 (2008) 135003.

[28] B. Qiao, M. Zepf, M. Borghesi, M. Geissler, Stable GeV ion-beam acceleration from thin foils by circularly polarized laser pulses, Phys. Rev. Lett. 102 (2009) 145002.

[29] M. Chen, A. Pukhov, T.P. Yu, Z.M. Sheng, Enhanced collimated GeV monoenergetic ion acceleration from a shaped foil target irradiated by a circularly polarized laser pulse, Phys. Rev. Lett. 103 (2009) 024801.

[30] T.P. Yu, A. Pukhov, G. Shvets, M. Chen, Stable laser-driven proton beam acceleration from a two-ion-species ultrathin foil, Phys. Rev. Lett. 105 (2010) 065002.

[31] S.C. Wilks, W.L. Kruer, M. Tabak, A.B. Langdon, Absorption of ultra-intense laser pulses, Phys. Rev. Lett. 69 (1992) 1383.

[32] J. Denavit, Absorption of high-intensity subpicosecond lasers on solid density targets, Phys. Rev. Lett. 69 (1992) 3052.

[33] A. Macchi, F. Cattani, T.V. Liseykina, F. Cornolti, Laser acceleration of ion bunches at the front surface of overdense plasmas, Phys. Rev. Lett. 94 (2005) 165003.

[34] A.P.L. Robinson, P. Gibbon, M. Zepf, S. Kar, R.G. Evans, et al., Relativistically correct hole-boring and ion acceleration by circularly polarized laser pulses, Plasma Phys. control. Fusion 51 (2009) 024004.

[35] T. Schlegel, N. Naumova, V.T. Tikhonchuk, C. Labaune, I.V. Sokolov, et al., Relativistic laser piston model: ponderomotive ion acceleration in dense plasmas using ultraintense laser pulses, Phys. Plasmas 16 (2009) 083103.

[36] F. Wagner, O. Deppert, C. Brabetz, P. Fiala, A. Kleinschmidt, et al., Maximum proton energy above 85 MeV from the relativistic interaction of laser pulses with micrometer thick CH_2 targets, Phys. Rev. Lett. 116 (2016) 205002.

[37] R. Kodama, K. Takahashi, K.A. Tanaka, M. Tsukamoto, H. Hashimoto, et al., Study of laser-hole boring into overdense plasmas, Phys. Rev. Lett. 77 (1996) 4906.

[38] S. Atzeni, J. Meyer-ter-Vehn, The Physics of Inertial Fusion: Beam Plasma Interaction, Hydrodynamics, Hot Dense Matter, Clarendon Press, Oxford, 2004.

[39] H. Hora, J. Badziak, M.N. Read, Y.T. Li, T.J. Liang, et al., Fast ignition by laser driven particle beams of very high intensity, Phys. Plasmas 14 (2007) 072701.

[40] S.M. Weng, M. Murakami, H. Azechi, J.W. Wang, N. Tasoko, et al., Quasi-monoenergetic ion generation by hole-boring radiation pressure acceleration in inhomogeneous plasmas using tailored laser pulses, Phys. Plasmas 21 (2014) 012705.

[41] J.J. Honrubia, J. Fernandez, B.M. Hegelich, M. Murakami, C.D. Enriquez, Fast ignition driven by quasi-monoenergetic ions: optimal ion type and reduction of ignition energies with an ion beam array, Laser Part. Beams 32 (2014) 419.

[42] J.J. Honrubia, M. Murakami, Ion beam requirements for fast ignition of inertial fusion targets, Phys. Plasmas 22 (2015) 012703.

[43] S. Eliezer, H. Hora, Double layers in laser-produced plasmas, Phys. Rep. 172 (1989) 339.

[44] H. Hora, Laser Plasma Physics, SPIE Press, 2016.
[45] S. Eliezer, N. Nissim, V. Martínez, M. José, K. Mima, et al., Double layer acceleration by laser radiation, Laser Part. Beams 32 (2014) 211−216.
[46] M. Murakami, H. Nagatomo, H. Azechi, F. Ogando, M. Perlado, et al., Innovative ignition scheme for ICF-impact fast ignition, Nucl. Fusion 46 (2006) 99−103.
[47] S.M. Weng, M. Liu, Z.M. Sheng, M. Murakami, M. Chen, et al., Dense blocks of energetic ions driven by multi-petawatt lasers, Sci. Rep. 6 (2016) 22150.
[48] X. Zhang, B. Shen, Z. Jin, L. Ji, Generation of plasma intrinsic oscillation at the front surface of a target irradiated by a circularly polarized laser pulse, Phys. Plasmas 16 (2009) 033102.
[49] X. Zhang, B. Shen, X. Li, Z.Y. Jin, F.C. Wang, et al., Efficient GeV ion generation by ultraintense circularly polarized laser pulse, Phys. Plasmas 14 (2007) 123108.
[50] S.M. Weng, P. Mulser, Z.M. Sheng, Relativistic critical density increase and relaxation and high-power pulse propagation, Phys. Plasmas 19 (2012) 022705.
[51] S.M. Weng, M. Murakami, P. Mulser, Z.M. Sheng, Ultra-intense laser pulse propagation in plasmas: from classic hole-boring to incomplete hole-boring with relativistic transparency, New J. Phys. 14 (2012) 063026.
[52] H. Xu, W. Yu, M.Y. Yu, A.Y. Wong, Z.M. Sheng, et al., Production of high-density high-temperature plasma by collapsing small solid-density plasma shell with two ultra-intense laser pulses, Appl. Phys. Lett. 100 (2012) 144101; High energy density micro plasma bunch from multiple laser interaction with thin target, Appl. Phys. Lett. 104, 024105(2014).
[53] S.S. Bulanov, E. Esarey, C.B. Schroeder, S.V. Bulanov, T. Zh, Esirkepov, et al., Enhancement of maximum attainable ion energy in the radiation pressure acceleration regime using a guiding structure, Phys. Rev. Lett. 114 (2015) 105003.
[54] K.V. Lezhnin, F.F. Kamenets, V.S. Beskin, M. Kando, T. Zh, Esirkepov, et al., Effect of electromagnetic pulse transverse inhomogeneity on ion acceleration by radiation pressure, Phys. Plasmas 22 (2015) 033112.
[55] A. Macchi, C. Benedetti, Ion acceleration by radiation pressure in thin and thick targets, Nucl. Instrum. Methods Phys. Res. A 620 (2010) 41.
[56] S. Kar, K.F. Kakolee, M. Cerchez, D. Doria, A. Macchi, et al., Experimental investigation of hole boring and light sail regimes of RPA by varying laser and target parameters, Phys. Rev. Lett. 109 (2012) 185006.
[57] Y.Q. Cui, W.M. Wang, Z.M. Sheng, Y.T. Li, J. Zhang, Quasimonoenergetic proton bunches generation from doped foil targets irradiated by intense lasers, Phys. Plasmas 20 (2013) 024502.
[58] S.M. Weng, M. Muramaki, Z.M. Sheng, Reducing ion energy spread in hole-boring radiation pressure acceleration by using two-ion-species targets, Laser Part. Beams 33 (2015) 103.
[59] X. Ribeyre, Ph Nicolaï, G. Schurtz, M. Olazabal-Loumé, J. Breil, et al., Compression phase study of the HiPER baseline target, Plasma Phys. control. Fusion 50 (2008) 025007.
[60] V.T. Tikhonchuk, T. Schlegel, C. Regan, M. Temporal, J.-L. Feugeas, et al., Fast ion ignition with ultra-intense laser pulses, Nucl. Fusion 50 (2010) 045003.
[61] A. Zani, D. Dellasega, V. Russo, M. Passoni, Ultra-low density carbon foams produced by pulsed laser deposition, Carbon 56 (2013) 358.
[62] C.S. Lau, J.A. Mol, J.H. Warner, G.A. Briggs, Nanoscale control of graphene electrodes, Phys. Chem. Chem. Phys. 16 (2014) 20398.
[63] G. Rydzek, Q.M. Ji, M. Li, P. Schaaf, J.P. Hill, et al., Electrochemical nanoarchitectonics and layer-by-layer assembly: from basics to future, Nano Today 10 (2015) 138.
[64] D.H.H. Hoffmann, V.E. Fortov, I.V. Lomonosov, V. Mintsev, N.A. Tahir, et al., Unique capabilities of an intense heavy ion beam as a tool for equation-of-state studies, Phys. Plasmas 9 (2002) 3651. D.H.H. Hoffmann, A. Blazevic, P. Ni, O. Rosmej, M. Roth, et al.; Present and future perspectives for high energy density physics with intense heavy ion and laser beams, Laser and Particle Beams 23, 47(2005).
[65] H. Hora, G.H. Miley, M. Ghoranneviss, B. Malekynia, N. Azizi, Laser-optical path to nuclear energy without radioactivity: fusion of hydrogen-boron by nonlinear force driven plasma blocks, Opt. Commmun. 282 (2009) 4124.
[66] H. Hora, G.H. Miley, M. Ghoranneviss, B. Malekynia, N. Azizi, et al., Fusion energy without radioactivity: laser ignition of solid hydrogen-boron (11) fuel, Energy Environ. Sci. 3 (2010) 479.
[67] S.M. Weng, Q. Zhao, Z.M. Sheng, W. Yu, S.X. Luan, et al., Extreme case of Faraday effect: magnetic splitting of ultrashort laser pulses in plasmas, Optica 4 (2017) 1086−1091.
[68] Y. Xu, J. Wang, X. Qi, M. Li, Y. Xing, et al., Improving the quality of proton beams via double targets driven by an intense circularly polarized laser pulse, AIP Adv. 6 (2016) 105304.
[69] Y. Xu, J. Wang, X. Qi, M. Li, Y. Xing, et al., Plasma block acceleration via double targets driven by an ultraintense circularly polarized laser pulse, Phys. Plasmas 24 (2017) 033108.
[70] M. Li, J.X. Wang, Y.X. Xu, W.J. Zhu, Study of plasma pressure evolution driven by strong picosecond laser pulse, Phys. Plasmas 24 (2017) 013117.
[71] D.A. Jones, E.L. Kane, P. Lalousis, P. Wiles, H. Hora, Density modification and energetic ion production at relativistic self-focusing of laser beams in plasmas, Phys. Fluids 25 (1982) 2295.
[72] L. Cicchitelli, H. Hora, R. Postle, Longitudinal field components for laser beams in vacuum, Phys. Rev. A 41 (1990) 3727.
[73] D. Umstadter, S.-Y. Chen, A. Maksimchuk, G. Mourou, R. Wagner, Nonlinear optics in relativistic plasmas and laser wake field acceleration of electrons, Science 273 (1996) 472−475.
[74] T. Häuser, W. Scheid, H. Hora, Acceleration of electrons by intense laser pulses in vacuum, Phys. Lett. A 186 (1994) 189−192.